

# A slender drop in a nonlinear extensional flow

Moshe Favelukis<sup>†</sup>

Department of Chemical Engineering, Shenkar – College of Engineering and Design,  
Ramat-Gan 5252626, Israel

(Received 22 March 2016; revised 23 July 2016; accepted 4 October 2016;  
first published online 2 November 2016)

The deformation of a slender drop in a nonlinear axisymmetric extensional and creeping flow has been theoretically studied. This problem, which was first suggested by Sherwood (*J. Fluid Mech.*, vol. 144, 1984, pp. 281–295), is being revisited, and new results are presented. The problem is governed by three dimensionless parameters: the capillary number ( $Ca \gg 1$ ), the viscosity ratio ( $\lambda \ll 1$ ), and the nonlinear intensity of the flow ( $E \ll 1$ ). Contrary to linear extensional flow ( $E = 0$ ), where the local radius of the drop decreases monotonically (in the positive  $z$  direction), in a nonlinear extensional flow ( $E \neq 0$ ), two possible steady shapes exist: steady shapes (stable or unstable) with the local radius decreasing monotonically, and steady shapes (unstable) where the local radius of the drop has a local maximum, besides the one at the centre of the drop. Similar to linear extensional flow, the addition of nonlinear extensional effects does not change the end shape of the steady drop, which has pointed ends. A stability analysis has been done to distinguish between stable and unstable steady shapes and to determine the breakup point. Time-dependent studies reveal three types of breakup mechanism: a centre pinching mode, indefinite elongation, and a mechanism that remind us of tip-streaming, where a cusp is developed at the end of the drop.

**Key words:** drops and bubbles, low-Reynolds-number flows, slender-body theory

## 1. Introduction

When a spherical drop of radius  $a$  and viscosity  $\mu_{in}$  is suspended in a surrounding fluid, of viscosity  $\mu$ , undergoing shear or extensional flow, it will deform. Assuming incompressible Newtonian fluids under creeping flow conditions, the problem is governed by two dimensionless parameters: the capillary number  $Ca = \mu Aa/\sigma$  and the viscosity ratio  $\lambda = \mu_{in}/\mu$ . Here  $A$  is the shear or extension rate and  $\sigma$  is the surface tension. At  $Ca \ll 1$ , the drop can be considered to be a slightly deformed sphere. However, in this report we shall consider slender drops only, which can be realized at  $Ca \gg 1$  and  $\lambda \ll 1$ . A summary of this fundamental research topic having many industrial applications can be found in excellent reviews by Rallison (1984), Stone (1994), and Briscoe, Lawrence & Mietus (1999).

Like many other topics in fluid mechanics, a slender-body theory for drops in creeping flow was first introduced by Taylor (1964). He considered the deformation of a slender drop in an axisymmetric linear extensional flow, where the cross-section

<sup>†</sup> Email address for correspondence: [favelukis@gmail.com](mailto:favelukis@gmail.com)

of the drop is circular. The theory, which was later refined by Buckmaster (1972, 1973), Acrivos & Lo (1978), Khakhar & Ottino (1986) and others, suggests that the slender drop has a parabolic radius profile with pointed ends. Consequently, as the capillary number increases, the drop becomes thinner, more elongated, and breaks at a critical value of  $Ca \lambda^{1/6} = 0.148$ . Thus, breakup is not possible for a bubble or an inviscid drop ( $\lambda = 0$ ) in axisymmetric linear extensional creeping flow.

Several theoretical variations to the problem of a slender drop in an extensional flow have been suggested in the literature. A slender drop in a two-dimensional extensional flow, a case where the drop cross-section is not circular, was studied by Hinch & Acrivos (1979). Evolution studies and breakup mechanisms of slender drops were treated by Hinch (1980) and Favelukis, Lavrenteva & Nir (2012). Since the Reynolds number based on the length of a long and slender drop may not be so small, Acrivos & Lo (1978) and Brady & Acrivos (1982) suggested the inclusion of weak inertial effects. Howell & Siegel (2004) investigated a slender non-axisymmetric drop. Booty & Siegel (2005) studied the effect of an insoluble surfactant on the surface of an inviscid slender drop. Finally, Favelukis & Nir (2001) and Favelukis, Lavrenteva & Nir (2005, 2006) included non-Newtonian effects outside and inside the drop, respectively.

One of the very interesting extensions to Taylor's theory (1964) can be found in the paper of Sherwood (1984), who included nonlinear terms in the extensional creeping flow and performed experiments showing the tip-streaming phenomenon. Note that today, the literature suggests that tip-streaming is caused by surfactants moving towards the tips of the drop and accumulating there (De Bruijn 1993; Janssen, Boon & Agterof 1994; Eggleton, Tsai & Stebe 2001; Renardy, Renardy & Cristini 2001). The formation of a pointed drop in a nonlinear two-dimensional extensional creeping flow was also considered by Antanovskii (1996), since it describes better (than the linear flow) the outer flow which occurs in Taylor's four-roller mill apparatus. It is the purpose of this report to revisit, present new results, and perform a complete stability analysis of the theoretical treatment of Sherwood (1984) on deformation and breakup of a slender drop in a nonlinear axisymmetric extensional creeping flow.

## 2. The governing equations

### 2.1. The flow outside the drop

Figure 1 shows a slender drop, positioned at the origin of a cylindrical coordinate system and embedded in an infinite incompressible Newtonian fluid, subjected to a nonlinear extensional creeping flow. The undisturbed motion suggested by Sherwood (1984) is given by

$$v_r = -\frac{1}{2}Ar - \frac{3}{2}Brz^2, \quad v_z = Az + Bz^3, \quad p = 3\mu B \left( z^2 - \frac{1}{2}r^2 \right). \quad (2.1a-c)$$

Here  $p$  is the pressure, which was defined in such a way that its value at the origin is set to zero. According to Sherwood (1984), quadratic terms were excluded in order to maintain the symmetry at  $z=0$ . When  $B=0$ , the well-known simple (linear) extensional flow is recovered. Note that we define extensional flow with  $A > 0$ ; however,  $B$  can take both positive or negative values.

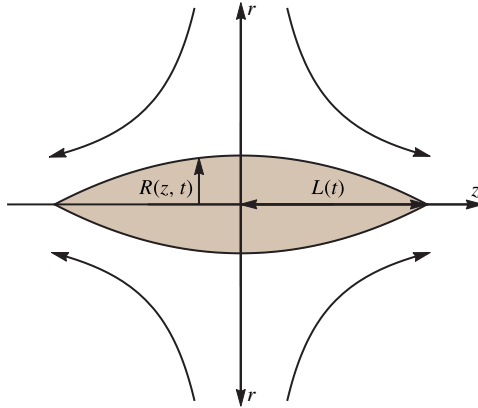


FIGURE 1. (Colour online) A slender drop in a nonlinear extensional flow:  $R(z, t)$  is the local radius and  $L(t)$  is the half-length of the drop.

Following Acrivos & Lo (1978), we can develop the velocity components of the disturbed motion near the slender drop:

$$\left. \begin{aligned} v_r &= \frac{R}{r} \frac{\partial R}{\partial t} + A \left\{ - \left( 1 + 3 \frac{B}{A} z^2 \right) \frac{r}{2} + \frac{R}{r} \left[ \left( 1 + 3 \frac{B}{A} z^2 \right) \frac{R}{2} + \left( 1 + \frac{B}{A} z^2 \right) z \frac{\partial R}{\partial z} \right] \right\}, \\ v_z &= Az \left( 1 + \frac{B}{A} z^2 \right). \end{aligned} \right\} \quad (2.2)$$

Notice that, to a first approximation, the axial component of the velocity is not affected by the presence of a slender drop. The radial disturbed velocity can be found from the continuity equation and the kinematic condition.

Substituting the disturbed motion into the Stokes equations, we find that the leading order of the pressure outside a slender drop ( $R/L \ll 1$ ) is

$$p_{out} = 3\mu Bz^2. \quad (2.3)$$

### 2.2. The flow inside the drop

The flow inside the slender drop can be considered to be a superposition of drag flow  $v_z$  at  $r=R$  and a pressure flow in the opposite direction (Taylor 1964). Assuming an incompressible Newtonian fluid in creeping flow we easily obtain

$$v_z = A \left( 1 + \frac{B}{A} z^2 \right) z - \frac{1}{4\mu_{in}} \frac{\partial p_{in}}{\partial z} R^2 \left[ 1 - \left( \frac{r}{R} \right)^2 \right]. \quad (2.4)$$

Here  $p_{in}$  is the pressure inside the drop, assumed uniform at each cross-section.

The volumetric flow rate, through each axial cross-section along the drop, can be found from an integral mass balance within a control volume inside the drop:

$$Q = - \frac{\partial}{\partial t} \int_0^z \pi R^2 dz = \int_0^R v_z 2\pi r dr = \pi R^2 \left[ A \left( 1 + \frac{B}{A} z^2 \right) z - \frac{1}{8\mu_{in}} \frac{\partial p_{in}}{\partial z} R^2 \right]. \quad (2.5)$$

From the last equation, and after some algebraic manipulation, an expression for the internal pressure can be found:

$$p_{in} = p_{in}(0) + 8\mu_{in}A \int_0^z \frac{1}{R} \left[ \left(1 + \frac{B}{A}z^2\right) \frac{z}{R} + \frac{1}{R^3} \frac{\partial}{\partial(At)} \int_0^z R^2 dz \right] dz, \tag{2.6}$$

where  $p_{in}(0)$  is the unknown pressure at the centre of the drop. At steady state, the volumetric flow rate vanishes at every cross-section within the drop. Also, for a bubble or an inviscid drop,  $\mu_{in} = 0$ , the pressure inside the drop is uniform, and at steady state it is also constant.

### 2.3. The normal stress balance

We start this section by writing a normal stress balance at the surface of the slender drop:

$$p_{in} - p_{out} - \tau_{rr,in} + \tau_{rr,out} = \frac{\sigma}{R}, \tag{2.7}$$

where the subscripts *in* and *out* denote inside and outside of the drop respectively. Since slender drops can be realized when the viscosity of the drop is much smaller than the viscosity of the external fluid, we can neglect the normal viscous stress inside the drop.

Let all the pressures and stresses be rendered dimensionless with respect to the characteristic stress outside the drop ( $\mu A$ ), all the lengths with respect to the equivalent radius ( $a$ , the radius of a sphere of an equal volume), and the time with respect to  $1/A$ . Substituting the expressions for the external and internal pressures, given by (2.3) and (2.6), and the external normal stress, which can be obtained from (2.2) and Newton’s viscosity law, we arrive in a dimensionless form:

$$p_{in}(0) + 8\lambda \int_0^z \frac{1}{R} \left[ (1 + Ez^2) \frac{z}{R} + \frac{1}{R^3} \frac{\partial}{\partial t} \int_0^z R^2 dz \right] dz - \frac{2}{R} \frac{\partial R}{\partial t} - 2 \left( 1 + \frac{9}{2} Ez^2 \right) - 2(1 + Ez^2) \frac{z}{R} \frac{\partial R}{\partial z} = \frac{1}{CaR}. \tag{2.8}$$

Equation (2.8) is governed by three dimensionless parameters: the capillary number, the viscosity ratio and the nonlinear intensity of the flow, which contrary to the other two parameters can be positive or negative:

$$Ca = \frac{\mu A a}{\sigma}, \quad \lambda = \frac{\mu_{in}}{\mu}, \quad E = \frac{Ba^2}{A}. \tag{2.9a-c}$$

The solution also requires three conditions: an initial drop shape:  $R(z, 0)$ , a radius at the end of the drop,  $R(L, t) = 0$ , and an equation for volume conservation:

$$\int_0^L R^2 dz = \frac{2}{3}. \tag{2.10}$$

Equations (2.8)–(2.10) suggest that  $R \sim O(1/Ca)$ ,  $L \sim O(Ca^2)$ ,  $p_{in}(0) \sim O(1)$ , and  $t \sim O(1)$ . In terms of the small parameter  $\varepsilon = R/L \ll 1$ , the theory is valid for large capillary numbers  $Ca \sim 1/\varepsilon^{1/3}$ , small viscosity ratios  $\lambda \sim \varepsilon^2$ , and a small nonlinear intensity of the flow  $E \sim \varepsilon^{4/3}$ . From the above discussion, and following

our previous report (Favelukis *et al.* 2006), we redefine the local radius and the coordinate  $z$  as follows:  $y = RCa$  and  $x = z/Ca^2$ , both having an order of magnitude of 1. Equations (2.8) and (2.10) take the following form:

$$p_{in}(0) + 8f^6 \int_0^x \frac{1}{y} \left[ (1 + Gx^2) \frac{x}{y} + \frac{1}{y^3} \frac{\partial}{\partial t} \int_0^x y^2 dx \right] dx - \frac{2}{y} \frac{\partial y}{\partial t} - 2 \left( 1 + \frac{9}{2} Gx^2 \right) - 2(1 + Gx^2) \frac{x}{y} \frac{\partial y}{\partial x} = \frac{1}{y} \tag{2.11}$$

$$\int_0^{x_L} y^2 dx = \frac{2}{3}, \tag{2.12}$$

with  $x_L = L/Ca^2$ . Note that the number of governing dimensionless parameters has been reduced from three ( $Ca, \lambda, E$ ) to two having an order of magnitude of 1: the positive viscous strength of the flow ( $f$ ) and the nonlinear strength of the flow ( $G$ ), which can be positive or negative:

$$f = Ca \lambda^{1/6}, \quad G = Ca^4 E. \tag{2.13a,b}$$

Following Hinch (1980), the pressure at the centre of the drop can be obtained by combining (2.11) and (2.12):

$$p_{in}(0) = 1 + \frac{\int_0^{x_L} \left( y + 2Gx^3 y \frac{\partial y}{\partial x} + 9Gx^2 y^2 \right) dx - 8f^6 \int_0^{x_L} y^2 \left\{ \int_0^x \frac{1}{y} \left[ (1 + Gx^2) \frac{x}{y} + \frac{1}{y^3} \frac{\partial}{\partial t} \int_0^x y^2 dx \right] dx \right\} dx}{\int_0^{x_L} y^2 dx}, \tag{2.14}$$

where, according to Hinch (1980), the numerical integration of the last equation, for the case of an inviscid drop in creeping flow, becomes unstable if the integral in the denominator is replaced, according to (2.12), by the value 2/3. We found this advice to be wise here and for our previous case as well (Favelukis *et al.* 2012).

The unknown internal pressure at the centre of the drop in (2.11) can be eliminated by differentiating the equation with respect to  $x$ , to give

$$2 \frac{\partial^2 y}{\partial x \partial t} - \frac{2}{y} \frac{\partial y}{\partial x} \frac{\partial y}{\partial t} + 2x(1 + Gx^2) \frac{\partial^2 y}{\partial x^2} - 2 \frac{x}{y} (1 + Gx^2) \left( \frac{\partial y}{\partial x} \right)^2 + \left[ 2(1 + 3Gx^2) - \frac{1}{y} \right] \frac{\partial y}{\partial x} + 18Gxy = 8f^6 \left[ \frac{x}{y} (1 + Gx^2) + \frac{1}{y^3} \frac{\partial}{\partial t} \int_0^x y^2 dx \right]. \tag{2.15}$$

The last equation needs to be solved with an initial drop shape,  $y(x, 0)$ , a vanishing drop radius at the end of the drop,  $y(x_L, t) = 0$ , and the conservation of volume, given by (2.12).

When  $G = 0$ , (2.15) reduces to the one presented in the literature for simple (linear) extensional flow. Furthermore, the  $18Gxy$  term (positive or negative) on the left-hand side of (2.15) reminds us of a similar term (negative) which needs to be added when external inertia is taken into account (Favelukis *et al.* 2006). Thus, we anticipate that some of the results of nonlinear extensional creeping flow, when  $G < 0$ , will be similar to those of linear extensional flow under the influence of a weak amount of external inertia.

In the next three sections we shall revisit the results of Sherwood (1984), for the steady deformation of inviscid and viscous drops, as well as present new contributions to this interesting subject.

3. Steady state

We start this section by examining the steady-state equation (2.15), which reveals an interesting finding. Contrary to the linear extensional flow case ( $G = 0$ ), where the local radius of the drop  $y(x)$  decreases monotonically, for  $z \geq 0$ , in a nonlinear extensional flow ( $G \neq 0$ ), the local radius of the drop may (or may not) achieve a maximum, besides the one at the centre of the drop.

3.1. The solution near the centre of the drop

At steady state, and according to (2.11), we shall follow the suggestion of Acrivos & Lo (1978) by defining the radius at the centre of the drop as follows:

$$y(0) = \frac{1}{2\nu}, \quad v = \frac{1}{2}p_{in}(0) - 1. \tag{3.1a,b}$$

Near the centre of the drop ( $x \rightarrow 0$ ), we assume that the local radius of the drop changes according to

$$y(x) = \frac{1}{2\nu} - \varepsilon(x), \quad \varepsilon(x) \ll 1. \tag{3.2}$$

Substituting the above definition into the steady-state equation (2.15) and neglecting terms of  $O(\varepsilon^2)$ , results, at a first approximation, in

$$-x \frac{d^2\varepsilon}{dx^2} + (\nu - 1) \frac{d\varepsilon}{dx} + \frac{9}{2\nu} Gx = 8\nu f^6 x. \tag{3.3}$$

Together with the condition that  $\varepsilon(0) = 0$  we obtain

$$\varepsilon = \frac{(16\nu^2 f^6 - 9G)x^2}{4\nu(\nu - 2)} + C \frac{x^\nu}{\nu}, \tag{3.4}$$

$$\frac{dy}{dx} = -\frac{(16\nu^2 f^6 - 9G)x}{2\nu(\nu - 2)} - Cx^{\nu-1}, \tag{3.5}$$

where  $C$  is an integration constant. The last two equations suggest that there is a singular point at  $\nu = 2$ . However, one should remember that  $\nu = 2$  corresponds to an inviscid drop ( $f = 0$ ) in linear ( $G = 0$ ) extensional flow. In this case, the last term on the left-hand side and the term on the right-hand side of (3.3) vanish, so that the first terms on the right-hand side of (3.4) and (3.5) do not exist. When  $\nu = 2$ , the solution is analytic, and we shall see later that  $C = 1/800$ . When  $\nu > 2$ , the last term on the right-hand side of (3.5) can be neglected when compared to the first term. If  $\nu < 2$ , the last term on the right-hand side of (3.5) is the leading one, suggesting a non-analytical solution at  $x = 0$ . However, following Acrivos & Lo (1978) for the case of an inviscid drop with external inertia, the coefficient of this non-analytical term can be made to vanish by a proper choice of  $\nu$ .

3.2. The solution near the end of the drop

Near the end of the drop ( $x \rightarrow x_L$ ), we assume a local radius profile of the form

$$y = M\varepsilon^\alpha, \quad \varepsilon = x_L - x \ll 1, \tag{3.6}$$

where both  $M$  and  $\alpha$  are defined as positive. Equation (3.6) suggests three possible shapes for the end of the slender drop: a cusped end ( $\alpha > 1$ ), a pointed end ( $\alpha = 1$ ) and a rounded end ( $\alpha < 1$ ). Substituting (3.6) into the steady-state equation (2.15) reveals that only the case  $\alpha = 1$ , where the end is pointed, is possible. This finding is equivalent to the linear extensional flow case, with or without a weak amount of external inertia (Favelukis *et al.* 2005, 2006).

At the end of the drop, the steady-state equation (2.15) reduces to

$$-2(1 + Gx^2)\frac{x}{y}\left(\frac{dy}{dx}\right)^2 - \frac{1}{y}\frac{dy}{dx} = 8f^6(1 + Gx^2)\frac{x}{y}. \tag{3.7}$$

Combining the last two equations (with  $\alpha = 1$ ) and applying a Taylor series for  $\varepsilon$  around  $\varepsilon = 0$  results in an algebraic equation, to which the first approximation solution is

$$M = \frac{1 \pm \sqrt{1 - 64f^6(x_L + Gx_L^3)^2}}{4(x_L + Gx_L^3)}, \quad \frac{dy}{dx} = -M. \tag{3.8a,b}$$

The following numerical results suggest that the (+) solution is the correct one. This might be expected when we explore (3.8) for the limiting case of an inviscid drop ( $f = 0$ ).

Despite the discussion presented here and in the previous section, one should remember that the slender-body approximation equations may not be accurate at the centre and at end of the drop.

#### 4. Inviscid drop ( $\lambda = 0$ )

##### 4.1. Steady-state shapes

For a bubble or an inviscid drop,  $\lambda = f = 0$ , the internal pressure is uniform and at steady state it is also constant. Combining the steady-state form of (2.11) with (3.1) results in

$$(1 + Gx^2)x\frac{dy}{dx} - \left(\nu - \frac{9}{2}Gx^2\right)y = -\frac{1}{2}. \tag{4.1}$$

The solution of (4.1) together with the boundary condition  $y(x_L) = 0$  requires a trial and error procedure in order to connect the parameters  $\nu$ ,  $x_L$  and  $G$  via the conservation of volume. The trial and error procedure can be avoided if one defines variables  $\theta = Gx^2$  and  $\theta_L = Gx_L^2$ , which can be positive or negative depending on the sign of  $G$ . With this definition, equation (4.1) and the conservation of volume, equation (2.12), become

$$2\theta(1 + \theta)\frac{dy}{d\theta} - \left(\nu - \frac{9}{2}\theta\right)y = -\frac{1}{2}, \tag{4.2}$$

$$G = \left(\frac{3}{4}\int_0^{\theta_L} y^2\theta^{-1/2} d\theta\right)^2. \tag{4.3}$$

For a choice of  $\nu$ ,  $\theta_L$  can be found by solving (4.2) from  $y(0) = 1/(2\nu)$  until  $y(\theta_L) = 0$ . Then, the parameter  $G$  can be obtained from the conservation of volume in (4.3).

An exact solution in a closed form can be found for (4.2) and its boundary condition at the end of the drop:

$$y = \frac{1}{4}(1 + \theta)^{-(\nu+9/2)/2}\theta_L^{-\nu/2} \left[ -(-\theta)^{\nu/2}\theta_L^{\nu/2}B[-\theta, -\nu/2, (\nu + 9/2)/2] + \theta^{\nu/2}(-\theta_L)^{\nu/2}B[-\theta_L, -\nu/2, (\nu + 9/2)/2] \right], \tag{4.4}$$

where  $B$  is the incomplete beta function defined by

$$B(z, a, b) = \int_0^z t^{a-1}(1 - t)^{b-1} dt. \tag{4.5}$$

Following Sherwood (1984), the solution can be obtained by expressing (4.2) as a power series in the form

$$y = \sum_{k=0}^{\infty} a_k \theta^k, \tag{4.6}$$

where the first few coefficients are given by

$$a_0 = \frac{1}{2\nu}, \quad a_1 = \frac{9}{4\nu(\nu - 2)}, \quad a_2 = \frac{117}{8\nu(\nu - 2)(\nu - 4)}. \tag{4.7a-c}$$

A general expression for the coefficients is

$$a_k = \frac{\prod_{j=0}^{k-1} (2j + 9/2)}{2 \prod_{j=0}^k (\nu - 2j)}. \tag{4.8}$$

For the specific case of  $j=0$ , the numerator is defined as 1. Note that  $\nu=0, 2, 4, 6, \dots$  are singular points and the solution contains many branches depending on values of  $\nu$ . Following Acrivos & Lo (1978) and Favelukis *et al.* (2006), we shall concentrate on solutions having low values of  $\nu$ , in the range  $0 < \nu < 4$ , as there we expect to find the stable solutions of physical interest.

Figure 2(a) shows the deformation curve of an inviscid drop for the range  $0 < \nu < 4$ , where 30 terms have been used in (4.6). First, let us observe the solid line, starting from the right-hand side of the plot at low  $\nu$ , large  $G$  and small  $x_L$ . As the parameter  $\nu$  increases, the positive  $G$  decreases and  $x_L$  increases, until we reach the case of an inviscid drop in creeping linear flow ( $\nu = 2, G = 0, x_L = 20$ ). Note that the literature suggests that an inviscid drop in linear extensional creeping flow is always stable and cannot be broken (Acrivos & Lo 1978). As the parameter  $\nu$  continues to increase, the solid line enters a region with negative values of  $G$ , which are very close to zero and therefore are difficult to observe in figure 2(a). The solid line turns back on itself at a bifurcation turning point ( $\nu = 2.51$ ), and finally terminates at  $\nu = 4, G = -0$  and  $x_L = 60.0$ . An enlargement of the turning point zone is depicted in figure 2(b).

Based on previous works (Acrivos & Lo 1978; Favelukis *et al.* 2006), steady stable shapes are probably located at the lower branch (low  $\nu$ ) until the bifurcation turning point at  $\nu = 2.51$ , while steady unstable shapes should be found at the upper branch



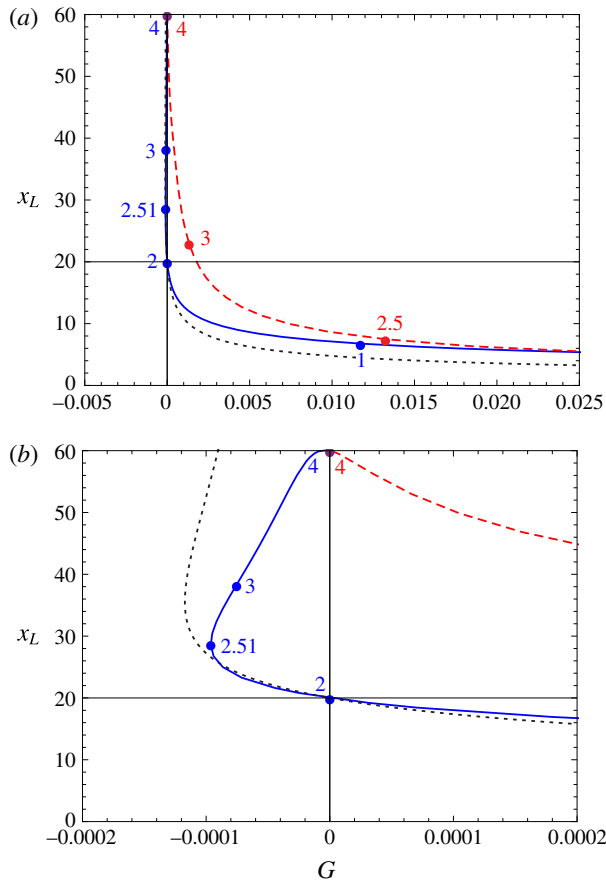


FIGURE 2. (Colour online) The deformation curve of an inviscid drop: (a) overall view; (b) enlargement of the turning point zone. Solid line:  $dy/dx < 0$  as  $x \rightarrow 0$  ( $x > 0$ ) with breakup point at  $\nu = 2.51$ ; dashed line:  $dy/dx > 0$  as  $x \rightarrow 0$  ( $x > 0$ ); dotted line: approximate solution. Solid circles are placed at different values of  $\nu$ .

and in other branches having higher values of  $\nu$  which are not plotted in this figure. At the bifurcation turning point, which is considered as the breakup point, the numerical results suggest  $\nu = 2.51$ ,  $G = -9.62 \times 10^{-5}$  and  $x_L = 28.7$ . We shall prove later, via a stability analysis, that our predictions are correct. Thus, contrary to the linear case ( $G = 0$ ), where the inviscid drop is always stable and breakup is not possible, the addition of nonlinear terms ( $G \neq 0$ ) can cause the bubble to break. The solid lines in figure 3 show steady shapes (stable or unstable) corresponding to the solid line of figure 2. Note that all cases have a local radius which decreases monotonically (for  $x \geq 0$ ), and when  $\nu < 1.68$ , the shapes also have an inflection point.

Next we discuss the dashed line in figure 2 which covers the range  $2 < \nu < 4$ . It starts at  $\nu$  just above 2 with large positive values of  $G$  and low values of  $x_L$ . As the parameter  $\nu$  increases,  $G$  decreases (always positive) and  $x_L$  increases, until the dashed line meets the solid line at  $\nu = 4$ ,  $G = +0$  and  $x_L = 60.0$ . At the centre of the slender drop,  $dy/dx = 0$ . Near the centre of the drop ( $x \rightarrow 0$ ) and if  $x$  is positive, equation (3.5) with  $f = 0$  suggests a negative slope,  $dy/dx < 0$ , for the solid line, and a positive slope,  $dy/dx > 0$ , for the dashed line. Therefore, the dashed line represents

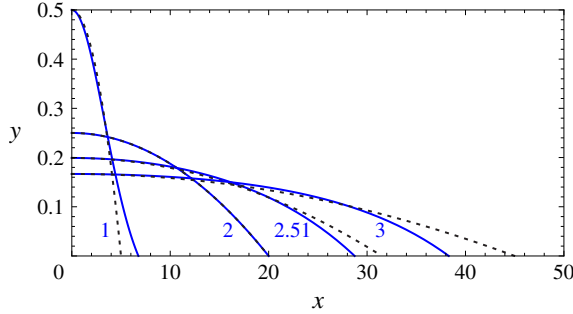


FIGURE 3. (Colour online) Steady-state shapes of inviscid drops, having  $dy/dx < 0$  as  $x \rightarrow 0$  ( $x > 0$ ), for different values of  $\nu$ . Solid lines: exact solution; dotted lines: approximate solution.  $\nu = 1$  (stable),  $\nu = 2$  (stable),  $\nu = 2.51$  (breakup point) and  $\nu = 3$  and (unstable).

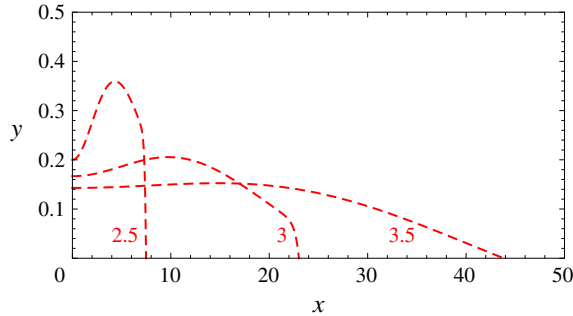


FIGURE 4. (Colour online) Steady-state shapes of inviscid drops, having  $dy/dx > 0$  as  $x \rightarrow 0$  ( $x > 0$ ), for different values of  $\nu$ , according to the exact solution. All cases are unstable.

steady shapes having a maximum in the local radius, besides the one at the centre of the drop (see figure 4). In the next section we shall prove through a stability analysis that these strange steady shapes are unstable. It should be noted that, contrary to the solid lines in figures 2 or 3, for these strange drops the numerical solution of the power series does not give a good prediction of the slope at the end of the drop, especially at the lower values of the parameter  $\nu$ .

An approximate solution can be obtained by considering the first two terms of (4.6). Together with the boundary condition at the end of the drop  $y(x_L) = y(\theta_L) = 0$ , and the conservation of volume, expressed by (2.12) or (4.3), we find that

$$y = \frac{1}{2\nu} \left[ 1 - \left( \frac{x}{x_L} \right)^2 \right], \quad x_L = 5\nu^2, \tag{4.9}$$

$$\theta_L = \frac{2(2-\nu)}{9}, \quad G = \frac{2(2-\nu)}{225\nu^4}. \tag{4.10a,b}$$

Notice that the two-term approximation suggests a parabolic radius profile; therefore, it cannot represent the unstable dashed line, which is characterized by having a maximum radius, besides the one at the centre. The two-term approximation is depicted in figure 2 by the dotted line. It closely follows the solid line, especially

when  $\nu > 2$ , and its bifurcation turning point is located at  $\nu = 8/3 = 2.67$ ,  $G = -1.17 \times 10^{-4}$  and  $x_L = 35.6$ . For the case of linear extensional flow ( $G = 0$ ), equation (4.9) also represents the exact solution after substituting  $\nu = 2$ , leading to  $x_L = 20$ . Steady shapes of deformed drops according to the approximate solution are represented by the dotted lines in figure 3. Despite the fact that the approximate solution underestimates the half-length of the drop when  $\nu < 2$  and overestimates the half-length at  $\nu > 2$  (see figure 3), it represents a simple and excellent alternative to the cumbersome numerical solution.

#### 4.2. The stability of the solution

In this section we perform a stability analysis to small disturbances of the steady shapes in order to find the location of the stable and unstable regions. For an inviscid drop  $f = 0$ , and (2.15) in terms of our new variable  $\theta = Gx^2$  takes the following form:

$$2 \frac{\partial^2 y}{\partial \theta \partial t} - \frac{2}{y} \frac{\partial y}{\partial \theta} \frac{\partial y}{\partial t} + 4(1 + \theta)\theta \frac{\partial^2 y}{\partial \theta^2} - 4 \frac{(1 + \theta)\theta}{y} \left( \frac{\partial y}{\partial \theta} \right)^2 + \left[ 4(1 + 2\theta) - \frac{1}{y} \right] \frac{\partial y}{\partial \theta} + 9y = 0. \tag{4.11}$$

Let a long-wave axisymmetric disturbance be defined as

$$y(\theta, t) = y_0(\theta) + y_1(\theta, t). \tag{4.12}$$

Here  $y_0$  is the steady-state solution and  $y_1$  is a time-dependent small axisymmetric perturbation such that  $y_1 \ll y_0$ . Combining the last two equations and neglecting terms of  $O(y_1^2)$  or higher we obtain

$$\begin{aligned} & 2 \frac{\partial^2 y_1}{\partial \theta \partial t} - \frac{2}{y_0} \frac{dy_0}{d\theta} \frac{\partial y_1}{\partial t} + 4(1 + \theta)\theta \frac{\partial^2 y_1}{\partial \theta^2} + \left[ 4(1 + 2\theta) - \frac{8(1 + \theta)\theta}{y_0} \frac{dy_0}{d\theta} - \frac{1}{y_0} \right] \frac{\partial y_1}{\partial \theta} \\ & + \left[ \frac{4(1 + \theta)\theta}{y_0^2} \left( \frac{dy_0}{d\theta} \right)^2 + \frac{1}{y_0^2} \frac{dy_0}{d\theta} + 9 \right] y_1 = 0. \end{aligned} \tag{4.13}$$

As always, the perturbation is described as  $y_1 = g(\theta) \exp(\delta t)$ , where negative real values of  $\delta$  denote stable steady shapes while positive real values of  $\delta$  denote unstable steady shapes. Thus, the point where the real part  $\delta$  vanishes can be considered as the breakup point. Substituting this definition into (4.13) gives

$$\begin{aligned} & 4(1 + \theta)\theta \frac{d^2 g}{d\theta^2} + \left[ 4(1 + 2\theta) + 2\delta - \frac{1}{y_0} - \frac{8(1 + \theta)\theta}{y_0} \frac{dy_0}{d\theta} \right] \frac{dg}{d\theta} \\ & + \left[ \frac{4(1 + \theta)\theta}{y_0^2} \left( \frac{dy_0}{d\theta} \right)^2 + \frac{1}{y_0^2} \frac{dy_0}{d\theta} + 9 - \frac{2\delta}{y_0} \frac{dy_0}{d\theta} \right] g = 0. \end{aligned} \tag{4.14}$$

We are looking for a solution to (4.14) in the form of a power series:

$$g(\theta) = \sum_{k=0}^{\infty} c_k \theta^k, \tag{4.15}$$

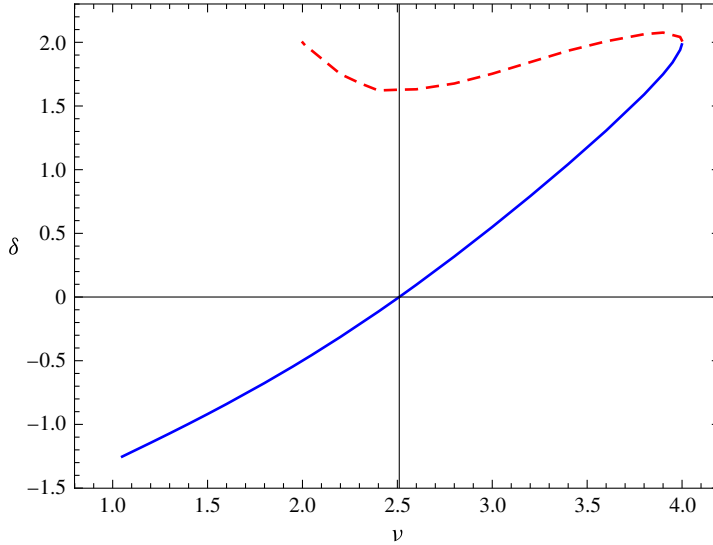


FIGURE 5. (Colour online) The stability of the solution of an inviscid drop. Solid line:  $dy_0/dx < 0$  as  $x \rightarrow 0$  ( $x > 0$ ), with breakup point at  $\nu = 2.51$ ; dashed line:  $dy_0/dx > 0$  as  $x \rightarrow 0$  ( $x > 0$ ).

where we set  $c_0 = 1$  without loss of generality (Acrivos & Lo 1978). We find for the first coefficients:

$$c_1 = \frac{9(2\nu - 2 - \delta)}{2(\nu - 2)(\nu - 2 - \delta)}, \quad c_2 = \frac{117[3\nu^2 - 3\nu(4 + \delta) + (2 + \delta)(4 + \delta)]}{4(\nu - 2)(\nu - 4)(\nu - 2 - \delta)(\nu - 4 - \delta)}. \quad (4.16a,b)$$

The conservation of volume, given by (2.12), can be differentiated with respect to time to give

$$\int_0^{x_L} y_0 y_1 \, dx = \int_0^{\theta_L} y_0 g \theta^{-1/2} \, d\theta = 0. \quad (4.17)$$

The eigenvalues  $\delta$  are determined by solving this last equation. For each  $\nu$  there are many possible values of  $\delta$ , and we are interested in  $\delta$  with the highest real part.

In figure 5 we show the highest real value of  $\delta$  as a function of the parameter  $\nu$  that was obtained with  $k = 12$  in (4.6) and (4.15). The solid and dashed lines in this figure correspond to the solid and dashed lines in figure 2, respectively. We find that for all cases  $\delta$  is real. As expected, the solid line ( $dy_0/dx < 0$ ,  $x \rightarrow 0$ ,  $x > 0$ ) contains both a stable region ( $\nu < 2.51$ ,  $\delta < 0$ ) and an unstable region ( $\nu > 2.51$ ,  $\delta > 0$ ), confirming our prediction that the breakup point ( $\delta = 0$ ) is located at the bifurcation turning point at  $\nu = 2.51$ . On the other hand, the dashed line ( $dy_0/dx > 0$ ,  $x \rightarrow 0$ ,  $x > 0$ ) represents an unstable physical situation ( $\delta > 0$ ) everywhere. It should be mentioned that  $\delta$  was found to be positive for all branches with  $\nu > 4$ , suggesting that no other steady stable shapes are expected.

#### 4.3. Time-dependent studies

In order to further confirm our stability analysis conclusions regarding the location of the stable and unstable steady shapes, here we shall perform a time-dependent study, which can also reveal the type of breakup mechanism. Following Sherwood (1984),

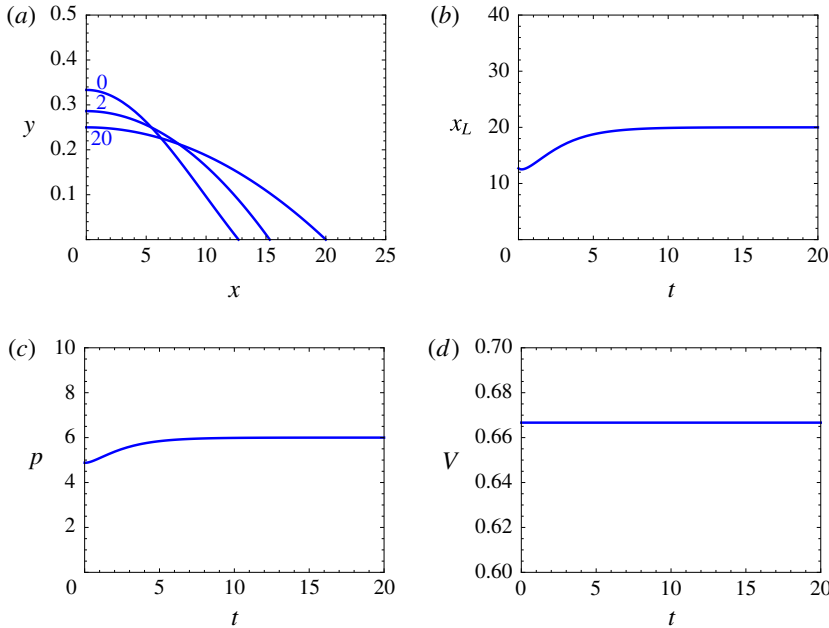


FIGURE 6. (Colour online) The evolution of an inviscid drop originally located at the stable branch with a sudden change in  $G$ . The drop is originally located at  $v = 1.5$ ,  $G = +0.00102$  and  $x_L = 12.7$ . At  $t = 0$   $G$  is changed to  $G = 0$  before the breakup point. (a) The local radius of the drop; (b) the half-length of the drop; (c) the pressure inside the drop; (d) the volume of the drop.

we suggest a solution for the evolution of the inviscid drop in terms of a series expansion about the centre of the drop:

$$y(x, t) = \sum_{k=0}^{\infty} y_k(t)x^{2k}, \tag{4.18}$$

which, after substitution into the partial differential (2.11) (with  $f = 0$ ), results in the following system of ordinary differential equations:

$$\frac{dy_0}{dt} = \frac{1}{2}[-1 + (p - 2)y_0]; \quad k = 0, \tag{4.19}$$

$$\frac{dy_k}{dt} = \frac{1}{2}[-(5 + 4k)Gy_{k-1} + (p - 2 - 4k)y_k]; \quad k \geq 1. \tag{4.20}$$

Note that for an inviscid drop the internal pressure is uniform and can be obtained from (2.14), with  $f = 0$ . Clearly, the accuracy of the solution depends on the maximum value of  $k$  used in (4.18). We used  $k = 15$  (16 terms) for figures 6 and 7, and the accuracy of the solution can be verified by the conservation of the volume. In all of the following simulations, we choose a stationary shape (stable or unstable) for the initial conditions.

In the first type of simulation experiments, we keep the nonlinear strength of the flow ( $G$  positive or negative) constant. If the inviscid drop is located at the stable

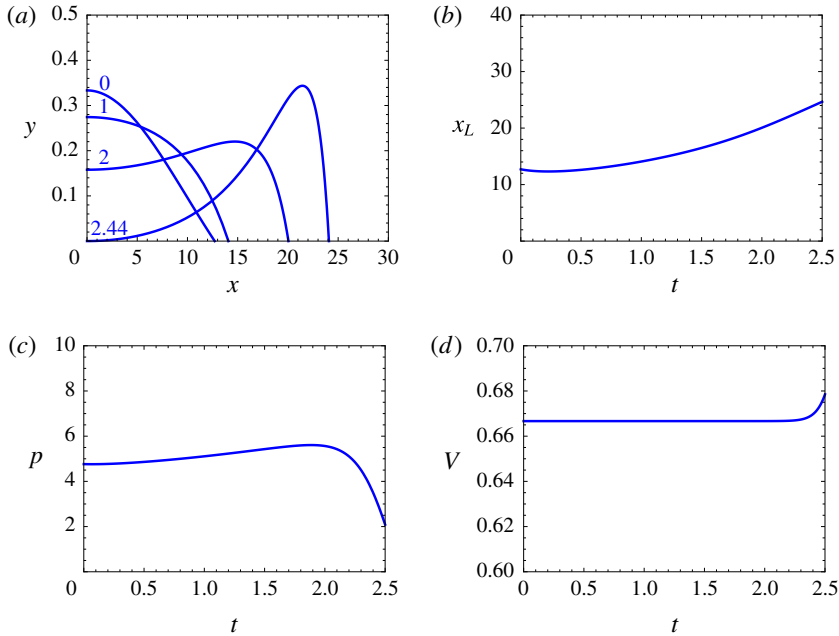


FIGURE 7. (Colour online) The evolution of an inviscid drop originally located at the stable branch with a sudden change in  $G$ . The drop is originally located at  $\nu = 1.5$ ,  $G = +0.00102$  and  $x_L = 12.7$ . At  $t = 0$   $G$  is changed to  $G = -0.001$  beyond the breakup point. (a) The local radius of the drop; (b) the half-length of the drop; (c) the pressure inside the drop; (d) the volume of the drop.

lower branch corresponding to  $\nu < 2.51$  ( $G$  positive or negative) and depicted in figure 2 by the solid line, no change in the drop is observed. On the other hand, if we place the drop at the unstable branch corresponding to  $2.51 < \nu < 4$  ( $G$  negative, solid line in figure 2), changes in the drop will occur with time. An example of such a case at  $\nu = 3$ ,  $G = -7.54 \times 10^{-5}$  and  $x_L = 38.3$  is presented in figure 12(d). Note that the steady inviscid drop is unstable and, after an incubation time, the drop breaks via a centre pinching mechanism. This mode of breakup mechanism has also been observed for the case of an inviscid drop under a small amount of external inertia (Favelukis *et al.* 2012). As we further increase the number of terms in (4.18), the initial steady shape is more accurate, and the evolution process takes longer. For this reason, in this type of simulation, no time is indicated.

The next type of simulation is what we call the Sherwood (1984) experiment. Here we study the evolution of the drop when at  $t = 0$  a sudden change in the nonlinear strength of the flow is introduced. Figures 6 and 7 correspond to an inviscid drop originally located at the steady stable branch at  $\nu = 1.5$ ,  $G = +0.00102$  and  $x_L = 12.7$ . In figure 6 we show the results of changing at  $t = 0$  the nonlinear strength of the flow from  $G = +0.00102$  to  $G = 0$ . As expected, the original stable drop moves to another stable location at  $\nu = 2$ ,  $G = 0$  and  $x_L = 20$ , corresponding to an inviscid drop in a linear extensional flow. Note that, contrary to the previous experiment depicted in figure 12(d), in this case we can indicate the times in our simulations. In figure 7, the change is made from  $G = +0.00102$  to  $G = -0.001$ , which is beyond the breakup point located at the bifurcation turning point at  $G = -9.62 \times 10^{-5}$ . As expected, breakup takes place, once again via a centre pinching mechanism.

5. Viscous drop ( $\lambda \neq 0$ )

We start this section by introducing a parameter characterizing the nonlinearity of the flow:

$$H = \frac{G}{f^6} = \frac{E}{\lambda Ca^2}. \tag{5.1}$$

Here  $-\infty < H < +\infty$ . When  $H = 0$  the linear extensional flow ( $G = 0$ ) is recovered, and  $H \rightarrow \pm\infty$  corresponds to an inviscid drop ( $f = 0$ ) under the influence of nonlinear ( $G \neq 0$ ) extensional effects.

Similar to our discussion in § 4.1, we define new variables  $\phi = f^6 x^2$  and  $\phi_L = f^6 x_L^2$ , which avoids the need of a trial and error solution. The governing equation, equation (2.15), and the conservation of volume, equation (2.12), take now the form

$$\begin{aligned} & 2 \frac{\partial^2 y}{\partial \phi \partial t} - \frac{2}{y} \frac{\partial y}{\partial \phi} \frac{\partial y}{\partial t} + 4(1 + H\phi)\phi \frac{\partial^2 y}{\partial \phi^2} - \frac{4(1 + H\phi)\phi}{y} \left( \frac{\partial y}{\partial \phi} \right)^2 \\ & + \left[ 4(1 + 2H\phi) - \frac{1}{y} \right] \frac{\partial y}{\partial \phi} + 9Hy \\ & = 4 \left[ \frac{(1 + H\phi)}{y} + \frac{1}{2\phi^{1/2}y^3} \frac{\partial}{\partial t} \int_0^\phi y^2 \phi^{-1/2} d\phi \right], \end{aligned} \tag{5.2}$$

$$f = \left( \frac{3}{4} \int_0^{\phi_L} y^2 \phi^{-1/2} d\phi \right)^{1/3}. \tag{5.3}$$

Note that, contrary to the inviscid case, where  $\theta$  can be positive or negative, this time  $\phi \geq 0$ .

5.1. Steady-state shapes

At steady state, the first two terms on the left-hand side and the last term on the right-hand side of (5.2) vanish. The solving procedure is identical to the one we applied for the inviscid drop. We first chose a value for the parameter  $\nu$ , and the end of the drop  $\phi_L$  can be evaluated by solving the steady form of (5.2) from  $y(0) = 1/(2\nu)$  until  $y(\phi_L) = 0$ . Finally, the parameter  $f$  is obtained from the conservation of volume given by (5.3).

As before, we are looking for a solution to the steady-state equation (5.2) in the form of a power series:

$$y = \sum_{k=0}^{\infty} b_k \phi^k \tag{5.4}$$

and the first few coefficients are

$$b_0 = \frac{1}{2\nu}, \quad b_1 = \frac{9H - 16\nu^2}{4\nu(\nu - 2)}, \quad b_2 = \frac{H[117H - 16\nu^2(11 + \nu)]}{8\nu(\nu - 2)(\nu - 4)}. \tag{5.5a-c}$$

Once again,  $\nu = 0, 2, 4, 6, \dots$  are singular points, the solution has many branches; we shall focus our search of the stable solution in the region of  $0 < \nu < 4$ .

Contrary to the inviscid case, for a viscous drop there are many possible solutions, depending on the combination of the parameters  $\nu$  and  $H$ . Therefore, and in order to facilitate the search, we will examine first the two-term approximate solution.

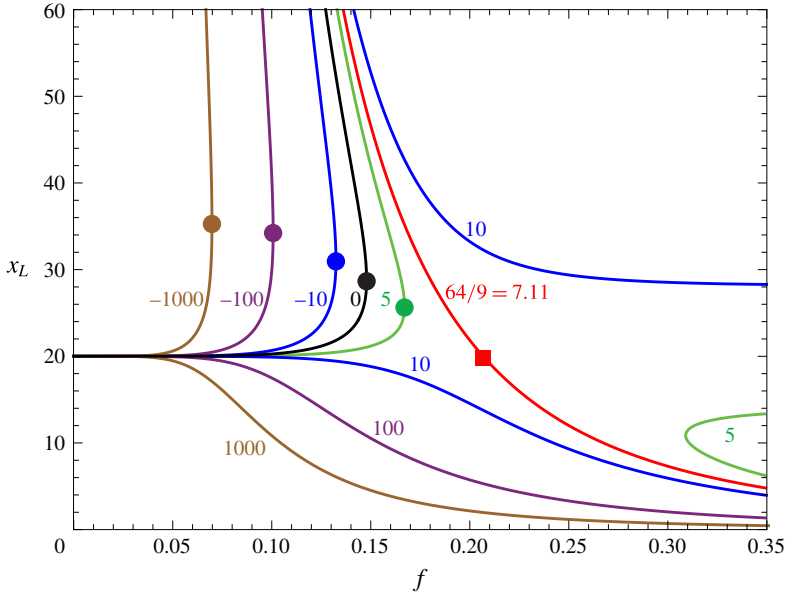


FIGURE 8. (Colour online) The deformation curve of viscous drops, according to the approximate solution, for different values of  $H$ . Solid circles are placed at bifurcation turning points. The solid square is placed at  $\nu = 2$ .

Taking the first two terms of (5.4) and applying the boundary condition at the end of the drop  $y(x_L) = y(\phi_L) = 0$ , and the conservation of volume, (2.12) or (5.3), we find

$$y = \frac{1}{2\nu} \left[ 1 - \left( \frac{x}{x_L} \right)^2 \right], \quad x_L = 5\nu^2, \tag{5.6}$$

$$\phi_L = \frac{2(\nu - 2)}{16\nu^2 - 9H}, \quad f = \frac{2^{1/6}}{5^{1/3}\nu^{2/3}} \left( \frac{\nu - 2}{16\nu^2 - 9H} \right)^{1/6}. \tag{5.7a,b}$$

As before, the two-term approximation suggests a parabolic radius profile with  $dy/dx < 0$  as  $x \rightarrow 0$  ( $x > 0$ ), and cannot represent possible shapes with  $dy/dx > 0$  as  $x \rightarrow 0$ , which, similar to the inviscid drop case, are probably unstable. Note that the two-term approximation equals the exact solution when the extensional flow is linear ( $H = 0$ ).

Figure 8 describes the deformation curve according to the approximate solution for different values of  $H$ . The figure can be divided into two regions: a region to the left of the  $H = 64/9 = 7.11$  line, having solutions for positive and negative values of  $H$ , and a region to the right of this curve, having solutions for positive values of  $H$  only.

To the left of the  $H = 64/9 = 7.11$  curve, we can locate the linear extensional case ( $H = 0$ ), where (5.6)–(5.7) also describes the exact solution, with  $2 \leq \nu < 2.4$  being the steady stable branch and  $\nu > 2.4$  the steady unstable branch. The breakup point located at the bifurcation turning point at  $\nu = 2.4$  is depicted by the solid circle. Other curves having  $H < 64/9$  (positive or negative),  $x_L > 20$  and  $\nu > 2$ , behave in a similar manner. That is, two branches separated by a bifurcation turning point at the solid circle. We can predict that the lower branch represents the steady stable shape and the upper branch represents the unstable steady shape.



$H$	$\nu$	$G$	$f$	$x_L$
$-\infty$	2.51	$-9.62 \times 10^{-5}$	0	28.7
-1000	2.51	$-9.53 \times 10^{-5}$	0.0676	28.7
-100	2.50	$-8.78 \times 10^{-5}$	0.0978	28.6
-10	2.44	$-4.95 \times 10^{-5}$	0.131	28.4
0	2.4	0	0.148	28.8
+1	2.39	$+1.18 \times 10^{-5}$	0.151	29.0

TABLE 1. Parameters at breakup point, according to the exact solution, for the family of solutions having:  $H < 64/9$  (positive or negative),  $x_L > 20$ ,  $\nu > 2$ , with bifurcation turning points.

To the left of the  $H = 64/9 = 7.11$  line, there is another family of solutions, corresponding to  $H > 64/9$ ,  $x_L < 20$  and  $\nu < 2$ . These curves remind us of the lower solid branch in figure 2 ( $G > 0$ ,  $\nu < 2$ ), which was found to be stable all along the curve; later we shall prove, via a stability analysis, that these curves are stable as well. Note that all lines to the left of the  $H = 64/9 = 7.11$  line concentrate to a single point at  $f = 0$  and  $x_L = 20$ , corresponding to an inviscid drop in linear extensional creeping flow ( $\nu = 2$ ).

To the right of the  $H = 64/9 = 7.11$  line, there are some curves presenting solutions for positive values of  $H$ , where cases having very large values of  $H$  exist, but cannot be shown as they are outside the range of the plot. These curves are located in a region in which the combination of the parameters  $H$  and  $\nu$  predicts, according to the exact solution, given by (3.5), that  $dy/dx > 0$  as  $x \rightarrow 0$  ( $x > 0$ ). Thus, all the curves to the right of the  $H = 64/9 = 7.11$  line are expected to be unstable.

Finally, the  $H = 64/9 = 7.11$  curve is actually composed of two branches. A lower branch ( $\nu < 2$ ,  $x_L < 20$ ) and an upper branch ( $\nu > 2$ ,  $x_L > 20$ ) merging at  $\nu = 2$ ,  $f = 0.207$  and  $x_L = 20$ , represented by the solid square. Clearly, this case cannot exist, since  $\nu = 2$  corresponds to an inviscid drop in linear extensional flow where  $f = 0$  and  $x_L = 20$ .

We now proceed to the exact solution represented by (5.4), calculated with  $k = 16$  and presented in figure 9. We start again with the family of curves corresponding to  $H < 64/9$  (positive or negative),  $x_L > 20$ ,  $\nu > 2$  and, according to (3.5),  $dy/dx < 0$  as  $x \rightarrow 0$  ( $x > 0$ ). Here we easily locate the linear extensional case ( $H = 0$ ), where the approximate solution is also the exact solution given by (5.6)–(5.7). To the left of  $H = 0$ , we find the solutions having  $H < 0$ . These curves behave in a very similar manner to the approximate solution. That is, two branches separated by a bifurcation turning point (solid circle). However, contrary to the approximate solution, the upper unstable branch does not extend to infinity, but rather turns back and ends up at  $f = 0$  and  $x_L = 60$ . To the right of the  $H = 0$  case we find some curves with  $H > 0$  but still under the  $H < 64/9$  condition. Some of these lines stop after the turning point ( $H = 1$ ) and some stop before the turning point is achieved ( $H = 5$ ). Later, our stability analysis will reveal that lines with bifurcation turning points are, as expected, stable at the lower branch and unstable at the upper branch, confirming that the turning point is the breakup point (see table 1). Lines without a bifurcation turning point, for example  $H = 5$ , are stable everywhere.

The next family of lines corresponds to  $H > 64/9$ ,  $x_L < 20$ ,  $\nu < 2$  and, according to (3.5),  $dy/dx < 0$  as  $x \rightarrow 0$  ( $x > 0$ ). These lines closely follow the approximate solution. However, it is difficult to determine the end point of these lines since, close to the end

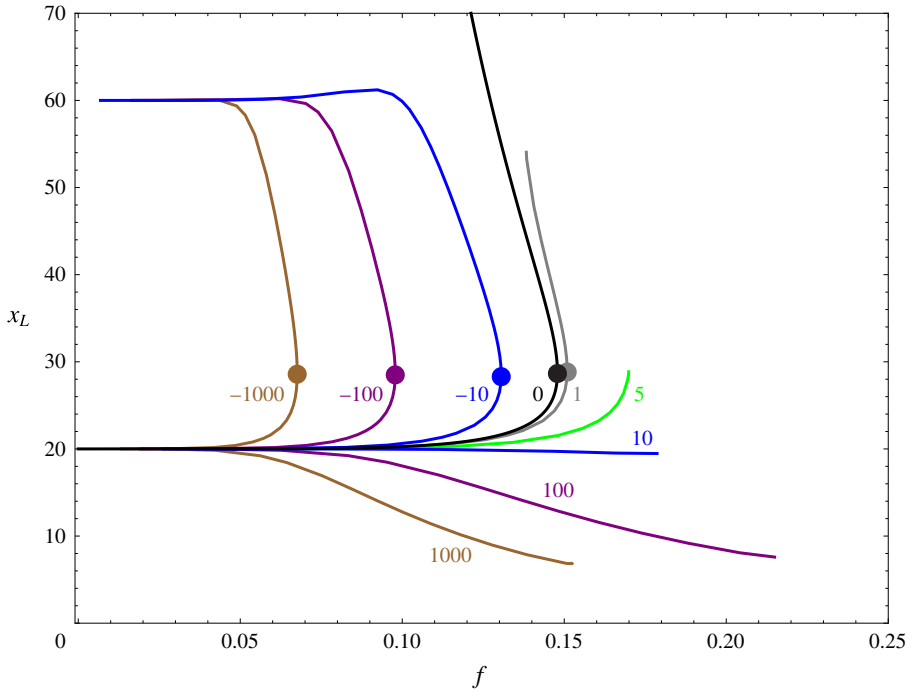


FIGURE 9. (Colour online) The deformation curves of viscous drops with  $dy/dx < 0$  as  $x \rightarrow 0$  ( $x > 0$ ), according to the exact solution, for different values of  $H$ . Solid circles are placed at bifurcation turning points.

points, the slope of the radius at the end of the drop, according to the series solution, deviates from the asymptotic value given by (3.8). Thus, we cannot conclude if these lines extend to infinity or they just stop as a result of our numerical procedure. The stability analysis in the next section will confirm that this family of curves is stable everywhere.

The third family of lines with  $H > 64/9$ ,  $\nu > 2$  and  $dy/dx > 0$  as  $x \rightarrow 0$  ( $x > 0$ ) is not shown in the figure. Remember that in this family the local radius of the drop achieves a maximum, besides the one at the centre of the drop; similar to the inviscid case, we expect this family to be unstable. Their numerical solution results in non-smooth lines in the deformation curve, and the slope of the radius at the end of the drop deviates completely from the asymptotic value given by (3.8).

Steady shapes (stable and unstable) for the two families of solutions with  $dy/dx < 0$  as  $x \rightarrow 0$  ( $x > 0$ ) are shown in figure 10. For comparison, the case of an inviscid drop in linear extensional flow ( $\nu = 2$ ,  $G = 0$ ) is also plotted. Drops having  $H = +100$  and  $\nu < 2$  are shorter and fatter than the  $\nu = 2$  case, and may have an inflection point, while for  $H = -100$  and  $\nu > 2$  they are longer and thinner than the  $\nu = 2$  case. Note also that the approximate solution closely follows the exact one. The approximate solution (compared at the same  $\nu$ ) underestimates the half-length of the drop when  $\nu < 2$  and overestimates the half-length at  $\nu > 2$ . However, since the approximate solution is represented by a very simple mathematical expression, it can provide an excellent tool for fast and practical estimations.

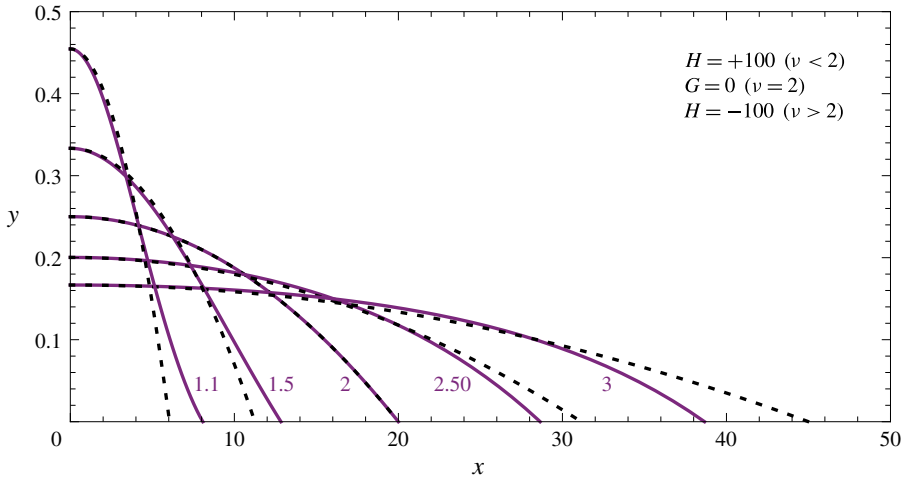


FIGURE 10. (Colour online) Steady-state shapes of inviscid and viscous drops with  $dy/dx < 0$  as  $x \rightarrow 0$  ( $x > 0$ ), for different values of  $\nu$ ,  $G$  and  $H$ . Solid lines: exact solution; dotted lines: approximate solution.  $\nu = 1.1$  and  $H = 100$  (stable),  $\nu = 1.5$  and  $H = 100$  (stable),  $\nu = 2$  and  $G = 0$  (stable),  $\nu = 2.50$  and  $H = -100$  (breakup point), and  $\nu = 3$  and  $H = -100$  (unstable).

### 5.2. The stability of the solution

We repeat the procedure used in the case of an inviscid drop by defining the steady solution  $y_0(\phi)$  and a small axisymmetric disturbance  $y_1(\phi, t)$ , such that

$$y(\phi, t) = y_0(\phi) + y_1(\phi, t), \tag{5.8}$$

which can be substituted into the governing (5.2) and by neglecting terms of  $O(y_1^2)$  or higher we obtain

$$\begin{aligned} & 2 \frac{\partial^2 y_1}{\partial \phi \partial t} - \frac{2}{y_0} \frac{dy_0}{d\phi} \frac{\partial y_1}{\partial t} + 4(1 + H\phi)\phi \frac{\partial^2 y_1}{\partial \phi^2} + \left[ 4(1 + 2H\phi) - \frac{8(1 + H\phi)\phi}{y_0} \frac{dy_0}{d\phi} - \frac{1}{y_0} \right] \frac{\partial y_1}{\partial \phi} \\ & + \left[ \frac{4(1 + H\phi)\phi}{y_0^2} \left( \frac{dy_0}{d\phi} \right)^2 + \frac{1}{y_0^2} \frac{dy_0}{d\phi} + 9H + \frac{4(1 + H\phi)}{y_0^2} \right] y_1 \\ & = \frac{4}{\phi^{1/2} y_0^3} \frac{\partial}{\partial t} \int_0^\phi y_0 y_1 \phi^{-1/2} d\phi. \end{aligned} \tag{5.9}$$

Setting  $y_1 = g(\phi) \exp(\delta t)$  into the last equation gives

$$\begin{aligned} & 4(1 + H\phi)\phi \frac{d^2 g}{d\phi^2} + \left[ 2\delta - \frac{8(1 + H\phi)\phi}{y_0} \frac{dy_0}{d\phi} + 4(1 + 2H\phi) - \frac{1}{y_0} \right] \frac{dg}{d\phi} \\ & + \left[ -\frac{2\delta}{y_0} \frac{dy_0}{d\phi} + \frac{4(1 + H\phi)\phi}{y_0^2} \left( \frac{dy_0}{d\phi} \right)^2 + \frac{1}{y_0^2} \frac{dy_0}{d\phi} + 9H + \frac{4(1 + H\phi)}{y_0^2} \right] g \\ & = \frac{4\delta}{\phi^{1/2} y_0^3} \int_0^\phi y_0 g \phi^{-1/2} d\phi. \end{aligned} \tag{5.10}$$

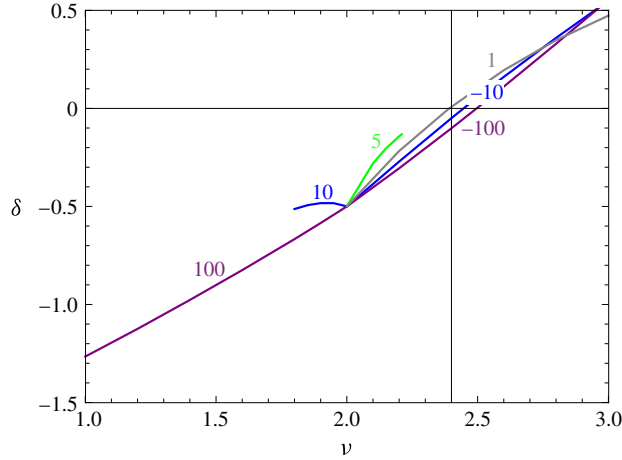


FIGURE 11. (Colour online) The stability of the solution of viscous drops with  $dy_0/dx < 0$  as  $x \rightarrow 0$  ( $x > 0$ ), for different values of  $H$ .

Let

$$g(\phi) = \sum_{k=0}^{\infty} d_k \phi^k, \tag{5.11}$$

where, once again,  $d_0 = 1$  and the next coefficient is

$$d_1 = \frac{9H(2\nu - 2 - \delta) - 16\nu^2[2 + (2\nu - 5)\delta]}{2(\nu - 2)(\nu - 2 - \delta)}. \tag{5.12}$$

Already the expression for  $d_2$  is so long that it is not presented here. The eigenvalues  $\delta$  are determined by solving the conservation of volume, given by (2.12), differentiated with respect to time:

$$\int_0^{x_L} y_0 y_1 dx = \int_0^{\phi_L} y_0 g \phi^{-1/2} d\phi = 0. \tag{5.13}$$

In figure 11 we show the highest real value of  $\delta$  as a function of the parameter  $\nu$ , obtained with  $k = 9$ , for the two families of lines plotted in figure 10 having  $dy/dx < 0$  as  $x \rightarrow 0$  ( $x > 0$ ), where we expect to find the stable steady shapes. We find that, for all cases, the largest  $\delta$  is real. As expected the stability analysis reveals that the family of curves corresponding to  $H < 64/9$  (positive or negative),  $x_L > 20$  and  $\nu > 2$  is stable at the lower branch and unstable at the upper branch, with the turning point being the breakup point and located at  $\delta = 0$ . Lines without a bifurcation turning point, such as  $H = 5$ , are stable everywhere. The other family of lines, having  $H > 64/9$ ,  $x_L < 20$ ,  $\nu < 2$ , is stable everywhere.

A few lines were omitted from figure 11 in order to make the figure more readable. Lines corresponding to  $H = \pm 1000$  do not appear since they are almost identical to the  $H = \pm 100$  lines. Also, the linear extensional case  $H = 0$  is absent since, at this range of  $\nu$ , it is almost identical to the  $H = 1$  line. Other cases with  $dy/dx > 0$  as  $x \rightarrow 0$  ( $x > 0$ ) that were not shown in figure 9 are also not shown here for the same reasons as discussed there. However, their non-smooth curves show positive values of  $\delta$ , predicting unstable steady shapes.

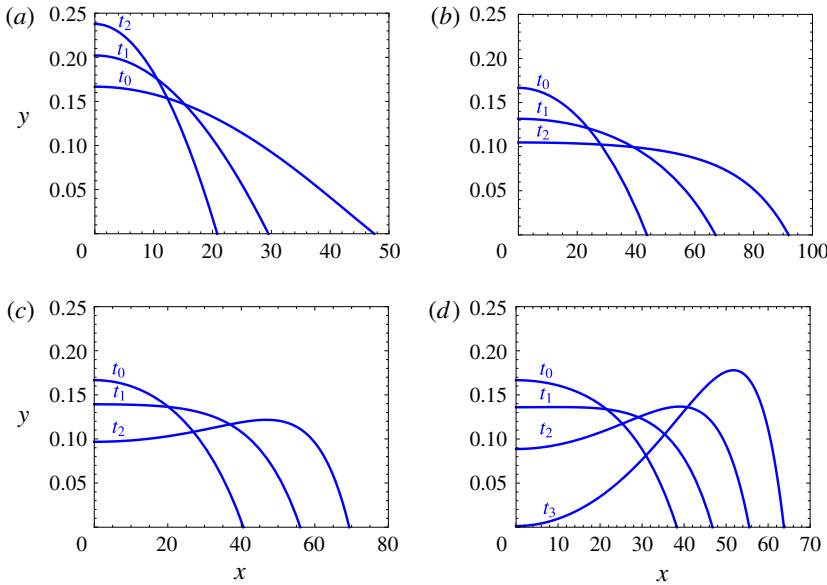


FIGURE 12. (Colour online) The evolution of inviscid and viscous drops originally located at the unstable branch with  $dy_0/dx < 0$  as  $x \rightarrow 0$  ( $x > 0$ ), with no change in  $G$  (inviscid drop) or  $f$  (viscous drop). At  $t=0$  all drops are located at  $v=3$ : (a)  $H=+1$ ; (b)  $H=-1$ ; (c)  $H=-10$ ; (d)  $H=-\infty$ .

5.3. Time-dependent studies

As before, we assume a solution to the evolution of the viscous drop in the form

$$y(x, t) = \sum_{k=0}^{\infty} y_k(t)x^{2k}. \tag{5.14}$$

But, contrary to the inviscid drop case, this time we find it more convenient to substitute the above equation into the differentiated governing equation, equation (2.15), to obtain

$$\frac{dy_0}{dt} = \frac{y_0[-4f^6 + 9Hf^6y_0^2 - y_1 + 2y_0(2y_1 + dy_1/dt)]}{8f^6 + 2y_0y_1}; \quad k=0, \tag{5.15}$$

where already the case  $k=2$  is so long that cannot be presented here. However, similar to (5.15), the  $dy_k/dt$  equation involves  $y_{k+1}$  and  $dy_{k+1}/dt$  terms. Thus, when choosing a maximum value of  $k=n$  for the simulations, we need to assume that  $y_{n+1}=0$ . We used  $n=6$  (7 terms) for the simulations, which were performed using Mathematica 9. Once again, stationary shapes (stable or unstable) were chosen for the initial conditions.

In figure 12(a–c), we explore viscous drops belonging to the family of solutions having  $H < 64/9$  (positive or negative),  $x_L > 20$  and  $dy/dx < 0$  as  $x \rightarrow 0$  ( $x > 0$ ). All cases in figure 12 are initially at  $v=3$ , which according to table 1 are beyond the bifurcation turning point and therefore represent steady unstable physical situations. In figure 12(a–c) (viscous drops) we keep the viscous strength of the flow ( $f$ ) constant; for comparison in figure 12(d) (inviscid drop), a case previously discussed,  $G$  was kept constant. As explained in § 4.3, in this type of simulation, exact values of the time are not indicated, as they depend on the number of terms used in (5.14).

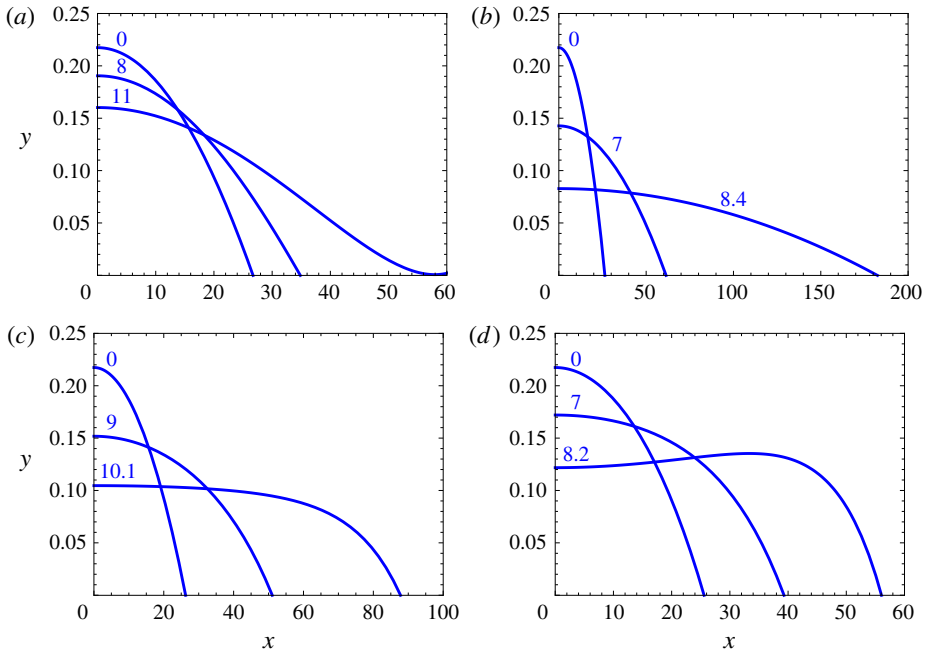


FIGURE 13. (Colour online) The evolution of viscous drops originally located at the stable branch with a sudden change in  $f$  beyond the breakup point. At  $t=0$  all drops are located at  $\nu=2.3$ : (a)  $H=+1$ ,  $f$  changes from 0.150 to 0.155; (b)  $H=0$ ,  $f$  changes from 0.147 to 0.155; (c)  $H=-1$ ,  $f$  changes from 0.144 to 0.150; (d)  $H=-10$ ,  $f$  changes from 0.129 to 0.135.

Figure 12(a), where  $H=+1$ , is very surprising. Originally the drop is located at the unstable branch at  $f=0.141$ , beyond the breakup point, with a half-length slightly smaller than  $x_L=50$  (see figure 9). As time passes, the drop does not break, but jumps down to the stable branch at the same  $f$  (since we kept it constant), but corresponding to a half-length slightly larger than  $x_L=20$ . The next two figures, figure 12(b,c), corresponding to negative values of  $H$ , are not so surprising, since we already mentioned below (2.15) that we anticipate some of the results of nonlinear extensional creeping flow, when  $G < 0$  ( $H < 0$ ), to be similar to those of linear extensional flow under the influence of a small amount of external inertia (Favelukis *et al.* 2012). According to Favelukis *et al.* (2012), at low values of external inertia (including a viscous drop in creeping flow) the breakup mechanism is indefinite elongation, while at larger values of inertia (including an inviscid drop) the mode of breakup is centre pinching. A similar picture is discovered here. At low values of the nonlinearity of the flow (for example, figure 12(b), where  $H=-1$  and  $f=0.136$ ), the drop breaks via an indefinite elongation mechanism; but when the nonlinearity of the flow is significant (for example, figure 12(c), where  $H=-10$  and  $f=0.123$ , or figure 12(d), with  $H=-\infty$  and  $f=0$ ), a centre pinching breakup mode is observed.

We continue with this family ( $H < 64/9$  positive or negative,  $x_L > 20$  and  $dy/dx < 0$  as  $x \rightarrow 0$  ( $x > 0$ )), and at  $t=0$  we introduce a sudden change in the viscous strength of the flow ( $f$ ). All cases in figure 13 start at  $\nu=2.3$ , representing steady stable drops (see table 1). Figure 13(a) corresponds to  $H=+1$ , where the bifurcation point is located at  $\nu=2.39$  and  $f=0.151$ . At  $t=0$ , the stable drop, located at  $\nu=2.3$  and  $f=0.150$ , is subjected to a sudden change to  $f=0.155$  beyond the breakup

point. Note that the breakup mechanism reminds us of tip-streaming, where a cusp is developed at the end of the drop. This mode of breakup was also reported by Sherwood (1984). In figure 13(b) we have a drop in linear extensional flow with  $H = 0$  and the sudden change is from  $\nu = 2.3$  and  $f = 0.147$  to  $f = 0.155$ . Here the breakup mode is by indefinite elongation, in accordance with previous studies (Sherwood 1984; Favelukis *et al.* 2012). Note that a breakup mechanism by indefinite elongation with no tip-streaming was experimentally observed by Bentley & Leal (1986) in a four-roll mill apparatus which produced a two-dimensional extensional flow. In their experiments the flow was near creeping, and the critical capillary number was less than one, while the condition for slender drops is  $Ca^3 \gg 1$ . Figure 13(c) corresponds to a small negative nonlinear contribution of  $H = -1$ , and the sudden change is from  $\nu = 2.3$  and  $f = 0.144$  until  $f = 0.150$ . As in figure 13(b), the breakup mechanism is by indefinite elongation, yet its shape, at long times, suggests a more uniform local radius than the linear case. Finally, in figure 13(d) a large negative nonlinear contribution of  $H = -10$  is studied. At  $t = 0$  the change is from  $\nu = 2.3$  and  $f = 0.129$  until  $f = 0.135$ , and breakup is by centre pinching.

## 6. Conclusions

The deformation and breakup of a slender drop in a nonlinear axisymmetric extensional and creeping flow has been the subject of this theoretical report. This interesting problem, which was first suggested by Sherwood (1984), is revisited, new results are presented, and a complete stability analysis is performed. The problem is governed by three dimensionless parameters: the capillary number ( $Ca \gg 1$ ), the viscosity ratio ( $\lambda \ll 1$ ), and the nonlinear intensity of the flow ( $E \ll 1$ ), which contrary to the other two parameters can be positive or negative. A further exploration of the governing equation shows that the number of dimensionless parameters can be reduced from three to two, both having an order of magnitude of 1: the viscous strength of the flow  $f = Ca \lambda^{1/6}$  and the nonlinear strength of the flow  $G = Ca^4 E$ .

When the extensional flow is linear ( $G = 0$ ), the literature suggests that the steady shape of the slender drop has a parabolic radius profile with pointed ends. As the capillary number increases, the drop becomes thinner and longer, and its surface area increases. Following Acrivos & Lo (1978), the radius at the centre of the drop is defined as  $1/(2\nu)$ , where  $\nu$  is related to the steady pressure at the centre of the drop. The steady deformation curve is composed of a stable branch at  $2 \leq \nu < 2.4$  and an unstable branch at  $\nu > 2.4$ , which are separated by a bifurcation turning (breakup) point. At this point  $\nu = 2.4$  and  $f = Ca \lambda^{1/6} = 0.148$ . Thus, it is not possible to break a bubble or an inviscid drop ( $\lambda = 0$ ,  $\nu = 2$ ) in linear extensional creeping flow.

The solution near the centre of the drop, together with a stability analysis, reveals that, contrary to the linear extensional flow case ( $G = 0$ ), where the local radius of the drop decreases monotonically (at  $z \geq 0$ ), in a nonlinear extensional flow ( $G \neq 0$ ), two possible steady shapes exist. Steady shapes (stable or unstable) with the local radius decreasing monotonically, and steady shapes (unstable) where the local radius of the drop achieves a maximum, besides the one at the centre of the drop. On the other hand, the solution close to the end of the drop suggests that steady slender drops with or without nonlinear effects have pointed ends.

Two types of solutions are presented for the case of an inviscid drop ( $\lambda = 0$ ) in a nonlinear ( $G \neq 0$ ) extensional creeping flow. A closed form involving the incomplete beta function and, as suggested by Sherwood (1984), a solution in the form of a power series, where here we suggest a simple and general expression for all the

coefficients. The deformation curve and the stability analysis reveal that the solution, where the local radius decreases monotonically, has the form of a lobe, composed of two branches, and separated by a bifurcation turning (breakup) point at  $\nu = 2.51$  and  $G = -9.62 \times 10^{-5}$ . In the first branch at  $\nu < 2$  and  $G > 0$ , and at  $2 < \nu < 2.51$  and  $G < 0$ , the solution is stable. The second branch at  $2.51 < \nu < 4$  and  $G < 0$  corresponds to unstable steady shapes. Steady shapes involving higher values of the parameter  $\nu$  are unstable. Thus, contrary to linear extensional flow, where an inviscid drop cannot be broken, the addition of nonlinear terms to the external flow can cause an inviscid drop to break.

Next, we considered the case of a viscous drop ( $\lambda \neq 0$ ) in a nonlinear ( $G \neq 0$ ) extensional creeping flow and find, as suggested by Sherwood (1984), that the solution is described as a power series. For simplicity we defined a parameter  $H = G/f^6$ , where  $H = 0$  corresponds to linear extensional flow ( $G = 0$ ), and  $H \rightarrow \pm\infty$  suggests a bubble or an inviscid drop ( $f = 0$ ) under the influence of nonlinear extensional effects. As before, we shall summarize our conclusions on steady shapes with the local radius decreasing monotonically, as there, according to the stability analysis, steady stable shapes were found. In the first family of solutions, corresponding to  $\nu > 2$  and  $H < 64/9$  (positive or negative), we find two types of deformation curves, with and without bifurcation turning points. As expected and validated by the stability analysis, lines with turning points are stable at the lower branch and unstable at the upper branch. Thus, the bifurcation turning point is the breakup point. Lines without a bifurcation turning point are always stable. The second family of lines, corresponding to  $\nu < 2$  and  $H > 64/9$ , is stable everywhere.

For both inviscid and viscous drops, we suggest approximate solutions by taking the first two terms of the exact power series solution. These solutions, having a parabolic radius profile, are equivalent to the exact solution when nonlinear effects are absent. Fortunately, the approximate solution, having a monotonically decreasing local radius, can predict steady shapes curves where stable shapes can be located. These solutions are found to be in excellent agreement with the exact results at the steady stable branch. Also, since they are represented by simple mathematical expressions, without performing heavy numerical calculations, they can provide excellent, fast and practical estimations for steady stable drop deformations.

Finally, time-dependent studies were performed for both inviscid and viscous drops where the local radius decreases monotonically ( $z > 0$ ). Two types of evolution simulations from originally steady (stable or unstable) drop shapes are presented: when the intensity of the flow was kept constant or was subjected to a sudden change. In agreement with Sherwood's (1984) report, the results here reveal three types of breakup mechanism: (i) a centre pinching mode for inviscid drops or viscous drops, both with large negative nonlinear effects ( $H \rightarrow -\infty$ ); (ii) indefinite elongation for viscous drops with zero or small negative nonlinear effects ( $H \rightarrow -0$ ); and (iii) a mechanism that remind us of tip-streaming, where a cusp is developed at the end of a viscous drop having relative small positive nonlinear effects ( $0 < H < 64/9$ ).

### Acknowledgement

This research was supported by Shenkar – College of Engineering and Design.

### REFERENCES

- ACRIVOS, A. & LO, T. S. 1978 Deformation and breakup of a single slender drop in an extensional flow. *J. Fluid. Mech.* **86**, 641–672.



- ANTANOVSKII, L. K. 1996 Formation of a pointed drop in Taylor's four-roller mill. *J. Fluid. Mech.* **327**, 325–341.
- BENTLEY, B.J. & LEAL, L. G. 1986 An experimental investigation of drop deformation and breakup in steady, two-dimensional linear flows. *J. Fluid Mech.* **167**, 241–283.
- BOOTY, M. R. & SIEGEL, M. 2005 Steady deformation and tip-streaming of a slender bubble with surfactant in an extensional flow. *J. Fluid Mech.* **544**, 243–275.
- BRADY, J. F. & ACRIVOS, A. 1982 The deformation and breakup of a slender drop in an extensional flow: inertial effects. *J. Fluid Mech.* **115**, 443–451.
- BRISCOE, B. J., LAWRENCE, C. J. & MIETUS, W. G. P. 1999 A review of immiscible fluid mixing. *Adv. Colloid Interface Sci.* **81**, 1–17.
- BUCKMASTER, J. D. 1972 Pointed bubbles in slow viscous flow. *J. Fluid. Mech.* **55**, 385–400.
- BUCKMASTER, J. D. 1973 The bursting of pointed drops in slow viscous flow. *J. Appl. Mech.* **E 40**, 18–24.
- DE BRUIJN, R. A. 1993 Tipstreaming of drops in simple shear flows. *Chem. Engng Sci.* **48**, 277–284.
- EGGLETON, C. D., TSAI, T.-M. & STEBE, K. J. 2001 Tip streaming from a drop in the presence of surfactants. *Phys. Rev. Lett.* **87**, 048302.
- FAVELUKIS, M., LAVRENTEVA, O. M. & NIR, A. 2005 Deformation and breakup of a non-Newtonian slender drop in an extensional flow. *J. Non-Newtonian Fluid Mech.* **125**, 49–59.
- FAVELUKIS, M., LAVRENTEVA, O. M. & NIR, A. 2006 Deformation and breakup of a non-Newtonian slender drop in an extensional flow: inertial effects and stability. *J. Fluid Mech.* **563**, 133–158.
- FAVELUKIS, M., LAVRENTEVA, O. M. & NIR, A. 2012 On the evolution and breakup of slender drops in an extensional flow. *Phys. Fluids* **24**, 043101.
- FAVELUKIS, M. & NIR, A. 2001 Deformation of a slender bubble in a non-Newtonian liquid in an extensional flow. *Chem. Engng Sci.* **56**, 4643–4648.
- HINCH, E. J. 1980 The evolution of slender inviscid drops in an axisymmetric straining flow. *J. Fluid Mech.* **101**, 545–553.
- HINCH, E. J. & ACRIVOS, A. 1979 Steady long slender droplets in two-dimensional straining motion. *J. Fluid Mech.* **91**, 401–414.
- HOWELL, P. D. & SIEGEL, M. 2004 The evolution of a slender non-axisymmetric drop in an extensional flow. *J. Fluid Mech.* **521**, 155–180.
- JANSSEN, J. J. M., BOON, A. & AGTEROF, W. G. M. 1994 Droplet break-up in simple shear flow in the presence of emulsifiers. *Colloids Surf. A* **91**, 141–148.
- KHAKHAR, D. V. & OTTINO, J. M. 1986 Deformation and breakup of slender drops in linear flows. *J. Fluid Mech.* **166**, 265–285.
- RALLISON, J. M. 1984 The deformation of small viscous drops and bubbles in shear flows. *Annu. Rev. Fluid. Mech.* **16**, 45–66.
- RENARDY, Y. Y., RENARDY, M. & CRISTINI, V. 2001 A new volume-of-fluid formulation for surfactants and simulations of drop deformation under shear at low viscosity ratio. *Eur. J. Mech. (B/Fluids)* **21**, 49–59.
- SHERWOOD, J. D. 1984 Tip streaming from slender drops in a nonlinear extensional flow. *J. Fluid Mech.* **144**, 281–295.
- STONE, H. A. 1994 Dynamics of drop deformation and breakup in viscous fluids. *Annu. Rev. Fluid. Mech.* **26**, 65–102.
- TAYLOR, G. I. 1964 Conical free surfaces and fluid interfaces. In *Proceedings of the 11th International Congress on Applied Mechanics, Munich*, pp. 790–796. Springer.